Chinese Chemical Letters 31 (2020) 1022–1025

Contents lists available at ScienceDirect

Chinese Chemical Letters

journal homepage: www.elsevier.com/locate/cclet

Communication

Ternary BiOBr/TiO_2/$Ti_3C_2T_x$ MXene nanocomposites with heterojunction structure and improved photocatalysis performance

Tianxiang Xu[a,b], Jiapei Wang[a,b], Ye Cong[a,b,*], Song Jiang[b], Qin Zhang[b], Hui Zhu[b], Yanjun Li[b], Xuanke Li[a,*]

[a] The State Key Laboratory of Refractories and Metallurgy, Wuhan University of Science and Technology, Wuhan 430081, China
[b] Hubei Province Key Laboratory of Coal Conversion and New Carbon Materials, Wuhan University of Science and Technology, Wuhan 430081, China

ARTICLE INFO

Article history:
Received 14 October 2019
Received in revised form 17 November 2019
Accepted 21 November 2019
Available online 21 November 2019

Keywords:
MXene
BiOBr
TiO_2
Heterojunction
Photocatalytic activity

ABSTRACT

The rational design and construction of heterojunction structure is an effective strategy to improve the photocatalytic performance. Herein, a series of BiOBr nanosheets-immobilized TiO_2/$Ti_3C_2T_x$ MXene hybrid materials with heterojunction structure were synthesized by a facial one-step hydrothermal method. The ternary composites show outstanding performance as photocatalysts for the degradation of rhodamine B due to the optimized synergetic effects of BiOBr, TiO_2 and $Ti_3C_2T_x$. The improved photocatalytic performance is remarkably attributed to the construction of a heterojunction between TiO_2 and BiOBr due to their well-matching of energy band position, which can enhance the absorption for visible light and promote the transfer of photo-generated charge carriers. Moreover, $Ti_3C_2T_x$ acts as an electron trap to further accelerate the separation of photo-generated electrons and holes.

With the growing problems of energy crisis and environmental pollution, solar energy utilization and conversion is crucial in the sustainable development of human society. Compared to the conventional treatment methods, photocatalytic oxidation technology using eco-friendly semiconductors has been regarded as a promising way to alleviate the worsening situation in environmental and energy, especially for treating pollutants in water [1–3]. Due to its natural abundance, non-toxicity, excellent chemical stability and photocatalytic activity, TiO_2 has been widely used as a semiconductor photocatalyst for organic pollutant degradation. However, the intrinsic wide band gap (~3.2 eV for anatase) leads to its activation only by ultraviolet light ($\lambda < 400$ nm), which greatly limits the practical applications of pure TiO_2 [4]. Therefore, many strategies have been developed to extend the light absorption range of TiO_2 into visible region, such as coupling TiO_2 with narrow bad gap semiconductors to form heterostructure. BiOBr is a good candidate for TiO_2 to form heterojunctions due to its suitable band gap (~2.7 eV) and chemical stability under visible light irradiation [5–7]. However, the general issue of rapid photo-generated electron-hole recombination still limits the further enhancement of photoactivity for BiOBr.

MXenes, an emerging two-dimensional materials family of early transition metal carbides and carbonitrides, have drawn widespread attention in the field of energy storage, environment remediation and biomedicine. Among the big MXene family, Ti_3C_2 MXene possesses the most in-depth etching chemistry and detailed theoretical research. Typically, the obtained multilayer Ti_3C_2 MXene is terminated by —OH, —O and/or —F functional groups (marked as T_x) and the formula is written as $Ti_3C_2T_x$ [8–10]. Owing to its high electrical conductivity, hydrophilicity and layered structure, $Ti_3C_2T_x$ is a promising cocatalyst in photocatalysis. Furthermore, $Ti_3C_2T_x$ can be used as an ideal precursor for the preparation of TiO_2/$Ti_3C_2T_x$ hybrid materials attributed to the uniformly dispersed titanium atoms [11–14]. But the multilayer morphology of $Ti_3C_2T_x$ affects the absorption of visible light and hinders the light capture by the photocatalyst, resulting in limited utilization of light and low photocatalytic activity [15]. Therefore, it is significant to reduce the thickness of $Ti_3C_2T_x$ and avoid preventing the light absorption of TiO_2.

Herein, 2D titanium carbide ($Ti_3C_2T_x$) nanosheets were firstly obtained by chemical exfoliation of commercially available Ti_3AlC_2 with lithium fluoride and hydrochloric acid. A series of ternary BiOBr/TiO_2/$Ti_3C_2T_x$ nanocomposites were successfully prepared by a facile one-step hydrothermal procedure (presented in the supporting information), which were recorded as BTM-*x* (*x* is the theoretical mass ratio of $Ti_3C_2T_x$ to BiOBr). For comparison, TiO_2/$Ti_3C_2T_x$ hybrids were synthesized *via* an *in-situ* oxidation of

* Corresponding authors at: The State Key Laboratory of Refractories and Metallurgy, Wuhan University of Science and Technology, Wuhan, 430081, China.
E-mail addresses: congye@wust.edu.cn (Y. Cong), lixuanke@wust.edu.cn (X. Li).

https://doi.org/10.1016/j.cclet.2019.11.038
1001-8417/

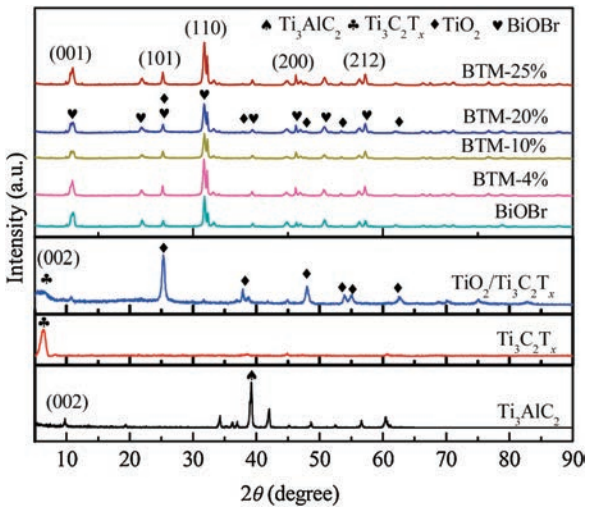

Fig. 1. XRD patterns of Ti_3AlC_2, $Ti_3C_2T_x$, $TiO_2/Ti_3C_2T_x$, BiOBr and $BiOBr/TiO_2/Ti_3C_2T_x$ composites.

the delaminated $Ti_3C_2T_x$ nanosheets and pure BiOBr was also obtained via the similar hydrothermal process. Detailed synthesis procedure, characterization and photocatalytic evaluation were given in the supplementary information. The morphology, crystal structure, optical property and visible-light photocatalytic activity of the as-synthesized composites were characterized by X-ray diffraction (XRD), scanning electron microscopy (SEM), high-resolution transmission electron microscopy (HRTEM), UV–vis diffuse reflectance spectra (UV–vis DRS), photoluminescence spectra (PL), respectively. Moreover, a possible photocatalytic mechanism of $BiOBr/TiO_2/Ti_3C_2T_x$ composites was proposed.

The X-ray diffraction patterns of pristine Ti_3AlC_2, $Ti_3C_2T_x$, $TiO_2/Ti_3C_2T_x$, BiOBr and $BiOBr/TiO_2/Ti_3C_2T_x$ composites were recorded in the 2θ range of 5°∼90° as illustrated in Fig. 1. After etching with lithium fluoride and hydrochloric acid, the characteristic diffraction peaks of Ti_3AlC_2 disappear. Meanwhile, the characteristic peaks according to (002) crystal plane is broadened and shifted from 9.8° to 6.2°, suggesting the successful exfoliation of Al atoms from the interlayers and the formation of $Ti_3C_2T_x$ MXene [16]. After *in situ* oxidation *via* hydrothermal process, several new diffraction peaks at $2\theta = 25.4°$, 37.9°, 48.2°, 54.1°, 55.2°, 62.9° emerge in $TiO_2/ Ti_3C_2T_x$, which are in good accordance with the (101), (004), (200), (105), (211) and (204) planes of the anatase phase of TiO_2 (JCPDS No. 73-1764), respectively. Besides, the diffraction peak ascribed to the (002) crystal plane of $Ti_3C_2T_x$ is still observable but presents relatively lower intensity than pristine $Ti_3C_2T_x$, which demonstrates the residue of $Ti_3C_2T_x$ MXene and part transformation to TiO_2 [17,18]. As shown in Fig. 1, typical peaks of the pure BiOBr were indexed as the tetragonal BiOBr (JCPDS No. 09-0393) without any crystalline impurity. For the $BiOBr/TiO_2/Ti_3C_2T_x$ composites, it can be observed that the co-exist of the diffraction peaks of BiOBr and TiO_2 in all the composites [19–21]. However, it is hard to observe any peaks of $Ti_3C_2T_x$, which may be explained by the relatively low content of $Ti_3C_2T_x$.

The morphology of the $Ti_3C_2T_x$, $TiO_2/Ti_3C_2T_x$, BiOBr and BTM-20% composites were characterized by SEM and HRTEM. Fig. 2a reveals the typical lamellar morphology of $Ti_3C_2T_x$ MXene, confirming the Ti_3AlC_2 was successfully exfoliated to form $Ti_3C_2T_x$ nanosheets. After the hydrothermal treatment, plenty of TiO_2 nanoparticles anchor on the $Ti_3C_2T_x$ sheets (Fig. 2b). As demonstrated in Figs. 2c and d, the smooth nanoplates of BiOBr are evolved into rough and covered with numerous TiO_2 nanoparticles on the surface of the BiOBr. The lamellar structure of BiOBr is retained during its coupling with $TiO_2/Ti_3C_2T_x$, which is consistent with the XRD results. HRTEM images of BTM-20% composites in Figs. 3a and b further show the distribution of TiO_2 and BiOBr in the hybrid composite$_2$. Combining with the HRTEM images and EDS elemental mappings of $BiOBr/TiO_2/Ti_3C_2T_x$ composites (Fig. S1 in Supporting information), it can be confirmed that the TiO_2 particles accompanied with residual $Ti_3C_2T_x$ lamella are distributed over the BiOBr lamella uniformly. As exhibition in Figs. 3c and d, the corresponding lattice fringe value of 0.35 nm and 0.28 nm coincides well with the (101) anatase crystal plane of TiO_2 and the (110) plane of BiOBr, respectively [22]. Combining with XRD results, it proves that there have realized ideal interfacial contact and construction of heterojunction between TiO_2 and BiOBr.

The UV–vis diffuse reflectance spectra (UV–vis DRS) and photoluminescence (PL) spectra were performed to analyze the optical properties of the as-synthesized nanocomposite. As shown in Fig. 4a, pure BiOBr exhibits a strong light response in ultraviolet region and its absorption edge for visible light is around 460 nm which corresponds to a band gap of 2.7 eV [23]. Meanwhile, $TiO_2/Ti_3C_2T_x$ shows higher visible absorption due to the essentially dark $Ti_3C_2T_x$. Compared with BiOBr, the UV–vis absorption edges of $BiOBr/TiO_2/Ti_3C_2T_x$ composites occur an obvious red shift and show enhanced absorption for visible light due to the synergistic effect between BiOBr and TiO_2. This means $BiOBr/TiO_2/Ti_3C_2T_x$ composites would be more effectively utilize solar energy than pure BiOBr, which is beneficial for improving photocatalytic efficiency.

To analyze the recombination details of photo-generated electrons and holes, room temperature PL spectra were carried out with an excitation wavelength of 325 nm. Fig. 4b shows the PL spectra of BiOBr, $TiO_2/Ti_3C_2T_x$ and $BiOBr/TiO_2/Ti_3C_2T_x$ composites. There is no doubt that $TiO_2/Ti_3C_2T_x$ and $BiOBr/TiO_2/Ti_3C_2T_x$ composites display much lower PL emission intensities than BiOBr, indicating their recombination of photo-generated electron-hole pairs is effectively inhibited [24]. It is rationally attributed by the remarkable conductivity of $Ti_3C_2T_x$ and band structure matching between BiOBr and TiO_2.

As shown in Fig. 4c, the photocatalytic activities of the as-prepared samples were evaluated by the degradation of rhodamine B solution (RhB, 100 mg/L) under visible light irradiation ($\lambda \geq 420$ nm). For eliminating the effect of absorption, all samples experienced a control test to get adsorption/desorption equilibrium in a dark condition before irradiation with visible light. It is obvious that

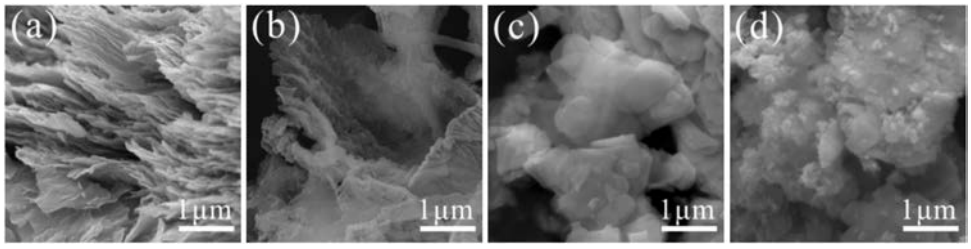

Fig. 2. SEM images of (a) $Ti_3C_2T_x$ (b) $TiO_2/Ti_3C_2T_x$ (c) BiOBr and (d) BTM-20%.

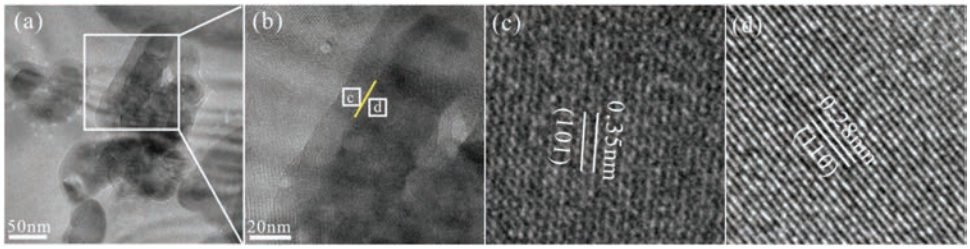

Fig. 3. (a, b) TEM images of BTM-20 %; (c, d) HRTEM of BTM-20%.

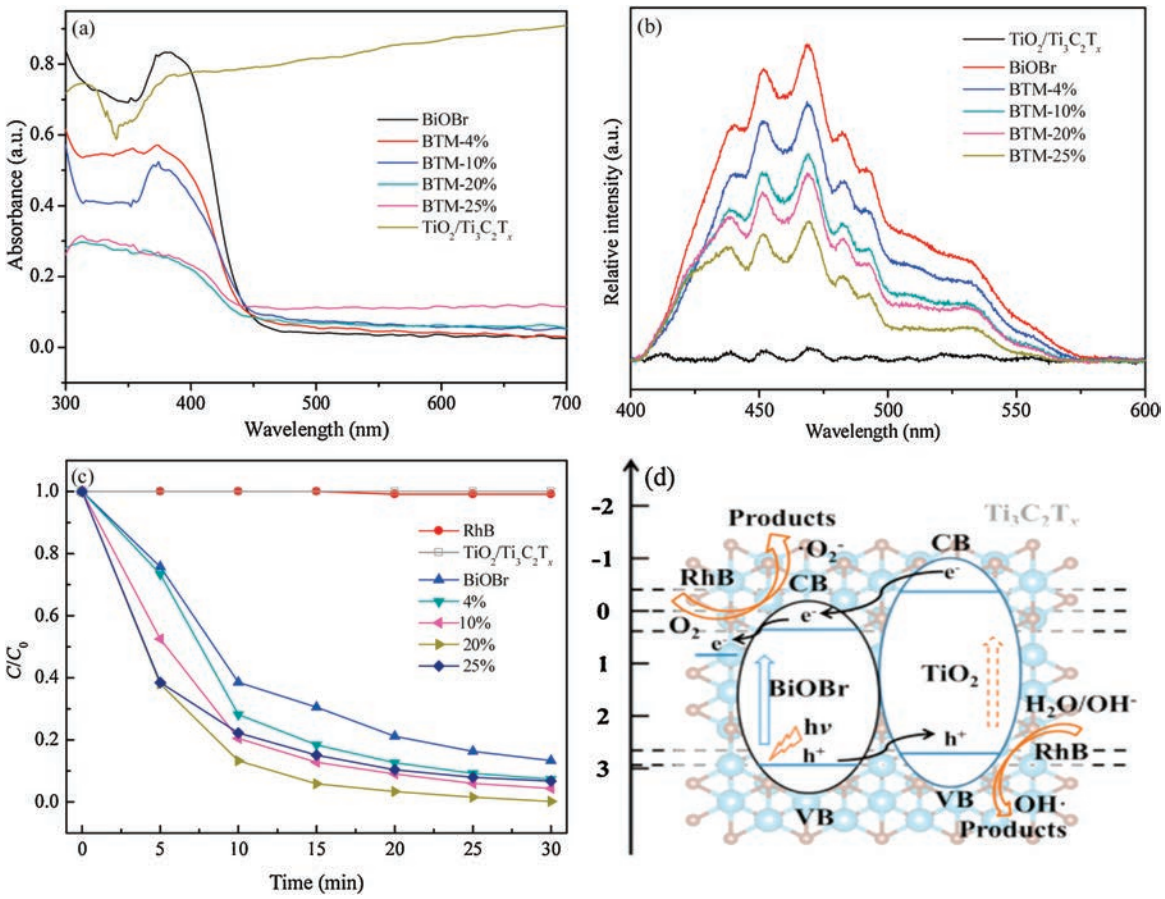

Fig. 4. (a) UV–vis DRS and (b) PL spectra of BiOBr, $TiO_2/Ti_3C_2T_x$ and $BiOBr/TiO_2/Ti_3C_2T_x$ composites. (c) Visible-light photocatalytic degradation of RhB solution over BiOBr, $TiO_2/Ti_3C_2T_x$ and $BiOBr/TiO_2/Ti_3C_2T_x$ composites. (d) The proposed charge separation and transfer pathways in the $BiOBr/TiO_2/Ti_3C_2T_x$ system under visible-light irradiation.

$TiO_2/Ti_3C_2T_x$ hybrids show barely photocatalytic activity for RhB under visible light irradiation within 30 min. Moreover, $BiOBr/TiO_2/Ti_3C_2T_x$ nanocomposites present higher photocatalytic activity than pure BiOBr and $TiO_2/Ti_3C_2T_x$, especially BTM-20% possesses 99.8% degradation rate for RhB within 30 min. Besides, the *x* value has a conspicuous effect on the photocatalytic activity and there is an optimal value. This is mainly due to the synergistic effects in the $BiOBr/TiO_2/Ti_3C_2T_x$ nanocomposites and ternary components play different roles in photocatalytic process. The recycling stability of BTM-20% during degradation of rhodamine B is presented in Fig. S3 (Supporting information). After five consecutive cycles, BTM-20% could keep 95.6% degradation rate, which indicates its good recyclability of the photocatalyst.

Based on the above results and discussion, a possible mechanism to explain the outstanding photocatalytic activity of $BiOBr/TiO_2/Ti_3C_2T_x$ nanocomposites is elucidated. On the one hand, the absorption edges of $BiOBr/TiO_2/Ti_3C_2T_x$ nanocomposites further extend to visible-light region and their absorption intensities enhance compared with BiOBr, which facilitates to harvest solar energy. On the other hand, the ternary heterojunction structure may generate a remarkable synergistic effect, leading to the efficient separation and transfer of photo-generated electrons and holes. As illustrated in Fig. 4d, the band gap of TiO_2 (~3.2 eV) is wider than that of BiOBr (~2.7 eV) and the corresponding conductive band (CB) and valence band (VB) positions of TiO_2 are both more negative than those of BiOBr. The intimate contact between BiOBr and TiO_2 may construct a heterojunction. As mentioned, TiO_2 shows only little visible light response due to its larger band gap, BiOBr can be excited easily by visible light and produce photo-induced electron-hole pairs. The construction of heterojunction between BiOBr and TiO_2 makes it rational that the photo-generated holes will rapidly migrate from the VB of BiOBr to VB of TiO_2 and the excited electrons will also transfer from the CB of TiO_2 to BiOBr under visible-light irradiation, leading to an

efficient separation and transfer of photo-generated electrons and holes [25]. What is more, the remaining $Ti_3C_2T_x$ in the ternary $BiOBr/TiO_2/Ti_3C_2T_x$ hybrids can serve as an efficient electron trap due to its intrinsic conductivity to further inhibit the photo-induced charge recombination [26]. The photo-generated electrons on the CB of BiOBr and TiO_2 will fast transfer to $Ti_3C_2T_x$. The holes accumulated in the valence band of TiO_2 possess outstanding ability to directly oxidize the pollutants adsorbed on the photocatalyst surface. Meanwhile, abundant holes can also react with OH^- groups and H_2O molecules to produce $^{\bullet}OH$ radicals. Superoxide radical anions ($^{\bullet}O_2^-$) may also emerge from the reaction of the electrons in the CB of BiOBr with oxygen molecules absorbed on the surface of materials or dissolved in water [27–30]. Subsequently, both $^{\bullet}OH$ and $^{\bullet}O_2^-$ could act as active species to effectively degrade RhB.

In this work, a series of ternary $BiOBr/TiO_2/Ti_3C_2T_x$ composites with heterojunction structure have been designed and constructed by a facile one-step hydrothermal process. The as-prepared ternary composites show higher visible-light photocatalytic activities for the degradation of RhB than pure BiOBr and $TiO_2/Ti_3C_2T_x$ due to the optimized synergetic effects of BiOBr, TiO_2 and $Ti_3C_2T_x$. It is found that there is a contact interface of heterojunction between BiOBr nanoplates and TiO_2 nanoparticles. The unique heterojunction structure not only enhance the absorption for visible light, but also promote the transfer of photo-excited electrons and holes due to the well-matching of energy band position between BiOBr and TiO_2. The introduction of $Ti_3C_2T_x$ serves as an efficient electron trap and accelerates the migration and transfer of photo-excited electrons. This work may provide reference of utilizing MXene as novel co-catalytic material to achieve highly efficient, steady and cost-effective semiconductor photocatalysts.

Declaration of competing interest

The authors declare that they have no known competing financial interests or personal relationships that could have appeared to influence the work reported in this paper.

Acknowledgments

This work was supported by the National Natural Science Foundation of China (Nos. 51472186, 51902232, 51402221) and the China Scholarship Council Fund (No. 201708420210).

Appendix A. Supplementary data

Supplementary material related to this article can be found, in the online version, at doi:https://doi.org/10.1016/j.cclet.2019.11.038.

References

[1] Z. Xing, J. Zhang, J. Cui, et al., Appl. Catal. B: Environ. 225 (2018) 452–467.
[2] T. Yang, J. Peng, Y. Zheng, et al., Appl. Catal. B: Environ. 221 (2018) 223–234.
[3] L. Lu, T. Jiang, W.S. Jing, G.W. Zhou, H.X. Shi, Chem. Lett. 47 (2018) 613–616.
[4] K. Qi, B. Cheng, J. Yu, W. Ho, Chin. J. Catal. 38 (2017) 1936–1955.
[5] C. Xue, T. Zhang, S. Ding, J. Wei, G. Yang, ACS Appl. Mater. Interfaces 9 (2017) 16091–16102.
[6] Z.D. Wei, R. Wang, Chin. Chem. Lett. 27 (2016) 769–772.
[7] M. Ji, Z. Zhang, J. Xia, et al., Chin. Chem. Lett. 29 (2018) 805–810.
[8] Z. Li, Y. Wu, Small (2019) 1804736.
[9] G. Gao, A.P. O'Mullane, A. Du, ACS Catal. 7 (2016) 494–500.
[10] Y. Yang, S. Umrao, S. Lai, S. Lee, J. Phys. Chem. Lett. 8 (2017) 859–865.
[11] K. Yan, Y. Guan, Y. Cong, et al., Chin. J. Inorg.Chem. 35 (2019) 1203–1211.
[12] B. Ahmed, D.H. Anjum, M.N. Hedhili, Y. Gogotsi, H.N. Alshareef, Nanoscale 8 (2016) 7580–7587.
[13] C. Peng, X. Yang, Y. Li, et al., ACS Appl. Mater. Interfaces 8 (2016) 6051–6060.
[14] X. Zhang, Y. Liu, S. Dong, Z. Ye, Y. Guo, Ceram. Int. 43 (2017) 11065–11070.
[15] W. Yuan, L. Cheng, Y. Zhang, et al., Adv. Mater. Interfaces 4 (2017) 1700577.
[16] J. Zhu, Y. Tang, C. Yang, F. Wang, M. Cao, J. Electrochem. Soc. 163 (2016) A785–A791.
[17] Y. Gao, L. Wang, A. Zhou, et al., Mater. Lett. 150 (2015) 62–64.
[18] C. Peng, H. Wang, H. Yu, F. Peng, Mater. Res. Bull. 89 (2017) 16–25.
[19] Q.X. Xia, N.M. Shinde, J.M. Yun, et al., Electrochim. Acta 271 (2018) 351–360.
[20] X. Yu, J. Shi, L. Feng, C. Li, L. Wang, Appl. Surf. Sci. 396 (2017) 1775–1782.
[21] T. Jiang, J. Li, Z. Sun, et al., Ceram. Int. 42 (2016) 16463–16468.
[22] J. Rashid, A. Abbas, L.C. Chang, et al., Sci. Total Environ. 665 (2019) 668–677.
[23] A.M. Alansi, M. Al-Qunaibit, I.O. Alade, T.F. Qahtan, T.A. Saleh, J. Mol. Liq. 253 (2018) 297–304.
[24] X. Li, C. Dong, K.L. Wu, et al., Mater. Lett. 164 (2016) 502–504.
[25] X. Tan, X. Li, T. Yu, Y. Zhao, Trans. Tianjin Univ. 22 (2016) 211–217.
[26] C. Liu, Q. Xu, Q. Zhang, et al., J. Mater. Sci. 54 (2019) 2458–2471.
[27] C. Xue, X. Xu, G. Yang, S. Ding, RSC Adv. 5 (2015) 102228–102237.
[28] W. Wang, Z. Zeng, G. Zeng, et al., Chem. Eng. J. 378 (2019) 122132.
[29] Y. Yang, Z. Zeng, G. Zeng, et al., Appl. Catal. B: Environ. 258 (2019) 117956.
[30] H. Yi, M. Jiang, D. Huang, et al., J. Taiwan Inst. Chem. E 93 (2018) 184–192.